Transcritical carbon dioxide heat pump cycle: Validation and comparison of one-dimensional models of ejector with independent data sets

Cong You, Benoit Michel, Rémi Revellin

Transcritical carbon dioxide heat pump cycle: validation and comparison of one-dimensional models of ejector with independent data sets

Cong You, Benoit Michel, Rémi Revellin

Univ Lyon, INSA Lyon, CNRS, CETHIL, UMR5008, 69621 Villeurbanne, France

Abstract

Two typical 1-D homogeneous equilibrium models from the literature (constant and variable pressure mixing models) were used to study the ejector expansion transcritical CO_2 heat pump cycle. A sensitivity analysis was performed to study the impact of the isentropic efficiency of the compressor and of each component of the ejector on the overall system performance. Two groups of independent experimental data from the literature were used to validate the two models. It was found that the cycle performance was more sensitive to the isentropic efficiency of the compressor than that of the individual components of the ejector. With appropriate input value of the compressor efficiency, both 1-D models accurately predicted the ejector outlet pressure and vapor quality. However, for the ejector entrainment ratio and cycle COP, the deviations were more than 50 %. These deviations can be significantly minimized to 10 % by eliminating the imbalance occurring in the system operation using a data post-processing method to correct the pseudo steady state in the real operation system. By comparing the simulation results of the two models, it has been shown that there is minor difference on the prediction accuracy. The research can serve as a practical reference for operation of two-phase-flow ejector expansion transcritical heat pump cycle, and can also provide an insight and orientation for the subsequent optimization of 1-D ejector numerical models.

Keywords: `Ejector`, Heat pump cycle, Carbon dioxide, Transcritical cycle, Experimental validation

Nomenclature

Acronyms

CFD computational fluid dynamics

CO_2 carbon dioxide

COP coefficient of performance

DEM delayed equilibrium model

GWP global warming potential

HEM homogeneous equilibrium model

HRM homogeneous relaxation model

$HVAC\&R$ heating, ventilation, air conditioning and refrigeration

IHX internal heat exchanger

ODP ozone depletion potential

Symbols

$\dot{m}$ mass flow rate [kg/s]

$\dot{Q}$ heat capacity [W]

$\dot{W}$ consumption power [W]

a section area [m^2]

h specific enthalpy [kJ/kg·K]

P pressure [MPa]

R relative performance ratio

T Temperature [°C]

u velocity [m/s]

w entrainment ratio of the ejector

x vapor quality

Greek Symbols

β liquid imbalance rate

ϵ tolerated deviation

η isentropic efficiency

ρ density [kg/m^3]

Subscripts

cal calculation value

$comp$ compressor

d diffuser

e evaporation

exp experimental data

gc, o	gas cooler outlet
is	ideal isentropic expansion or compression
m	motive flow at the ejector inlet
mix	mixed flow
s	suction flow at the ejector inlet
sh	super heat
$unit$	unit mass flow rate

1. Introduction

Heat pumps represent the most efficient alternative to fuel combustion and electric systems in the field of heating, ventilation, air conditioning and refrigeration (HVAC&R). Compared to systems based on combustion processes, heat pumps are cheaper and safer for operation. The life-span of heat pumps is relatively long with less maintenance (the average life-span is between 14 to 15 years [1]), which means they are exceptionally reliable source of heating and cooling. During the last decades, the overuse of traditional refrigerants in the HVAC&R systems exacerbated environmental and climate degradation [2]. As being a natural fluid with excellent thermo-physical properties, CO_2 is a promising working fluid to replace the traditional refrigerants. It presents the advantage of having a negligible impact on climate change, with zero ODP (Ozone Depletion Potential) and 1 GWP (Global Warming Potential), it is non-toxic, non-flammable and non-corrosive [3]. In addition, CO_2 can also be used in the transcritical heat pump system to improve the cycle efficiency due to the advantage of the temperature range.

However, for the traditional CO_2 cycles with throttling valve as an expansion device, there is a significant amount of irreversibilities that occurs in the expansion process, resulting in the decrease of cycle COP (Coefficient of Performance). The irreversibilities are even more pronounced in the transcritical CO_2 cycle, as the pressure ratio of the expansion is higher than that of other fluids such as R134a, R245fa or R1233zd. Cycle modification to replace the expansion valve for performance enhancement is a promising research domain nowadays [2].

Applied in the heat pump cycle to replace the traditional expansion valve, ejectors can reduce the throttling loss and expansion irreversibility. A typical schematic of the CO_2 ejector expansion heat pump cycle and corresponded pressure-enthalpy diagram are depicted in Fig.1. The main components in the cycle are the compressor, the gas cooler, the ejector, the vapor-liquid separator, the expansion valve and the evaporator. The auxiliary pipes and valves are not presented in the diagram. Compared to the traditional heat pump cycle, the ejector replaces the expansion valve to recover the expansion energy.

From Fig. 1, the refrigerant at state 1 is compressed into a supercritical fluid (state 2) in the compressor, then cooled down in the gas cooler (state 3). After expansion in the ejector, the main flow is divided into saturated vapor and saturated liquid in the separator (state 1 and 7). The saturated liquid then flows through

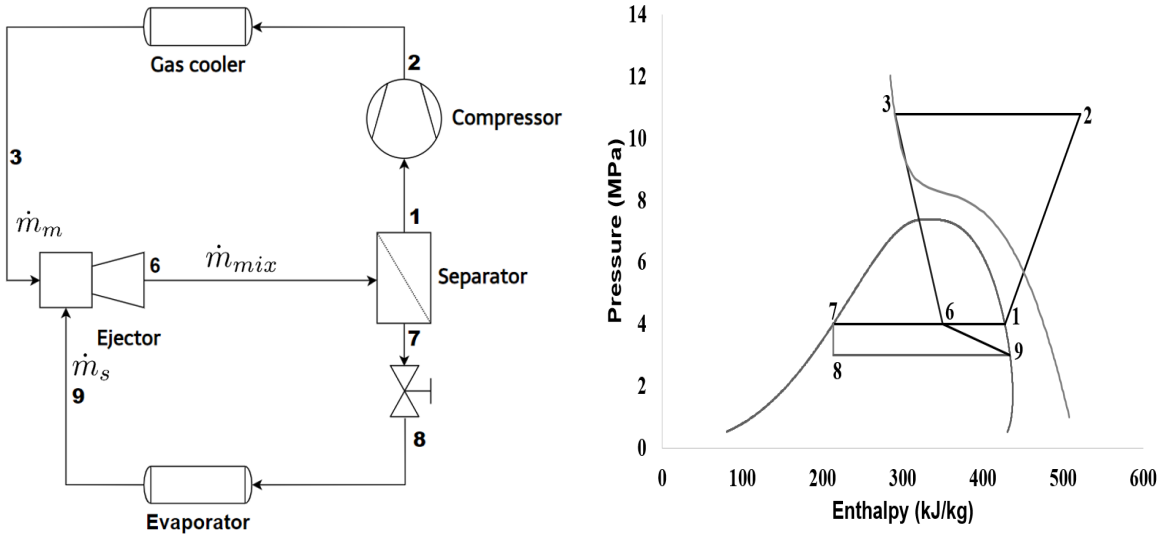

(a) (b)

Figure 1: (a) Schematic of the ejector expansion cycle (b) Corresponding $P-h$ diagram

the expansion valve (state 8) and enters the evaporator. After evaporation (state 9), the vapor from the evaporator is entrained at the inlet of ejector and then a complete loop is accomplished.

The ejector is the most important component of the cycle and the research on ejectors are focused on the following topics: parameter optimization, structural design, simulation and experimental validation [4–7]. As shown in Fig. 2, the ejector is generally divided into four sections, namely the driving and suction nozzles, the constant–area mixing section and the diffuser section. The motive flow, also named primary flow (supercritical liquid), accelerates in the driving nozzle and expands from the high pressure P_3 to the low pressure P_4. The suction flow (or secondary flow) accelerates and slightly expands (the expansion is ignored in some studies [8–10]) from P_9 to P_4 in the suction nozzle. The two streams then enter and mix up in the constant-area mixing section. The mixed flow decelerates and is pressurized to an intermediate pressure P_6 in the diffuser afterwards. The mass flow ratio of the suction flow and the motive flow entering the ejector is defined as the entrainment ratio (w) of the ejector (Eq. 1).

$$w = \dot{m}_s/\dot{m}_m \tag{1}$$

The inlet pressure of the compressor raises from the evaporation pressure to a higher value by the ejector, contributing to less compression work and to the improvement of the system's COP. To study the complicated thermohydraulic mechanisms inside the ejector or to quickly get the predicted values of the ejector's outlet parameters, numerous scholars have made attempts to simulate the flow inside ejectors [8, 9, 11–22]. Generally, the simulation models can be classified into two groups: zero/one-dimension-models and two/three-dimension-models.

A two/three-dimension computational fluid dynamics (CFD) model is more complex. Moreover the meshing and model solving is more time consuming. However, CFD models are more accurate in reflecting the internal

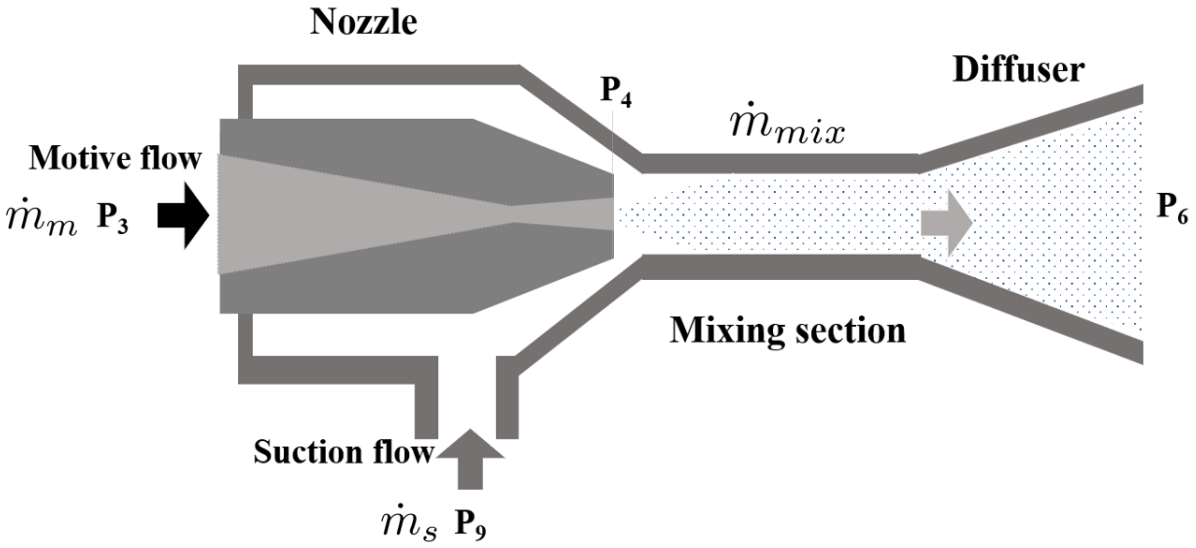

Figure 2: Structure of an ejector

two-phase flow inside the ejector. With the CFD simulation method, it is possible to obtain comprehensively observation of the flow inside the ejector and to optimise its design [11]. Zero/one-dimension-models are simpler and less costly than CFD techniques since they require no complex meshing. The first one-dimension-model was introduced by Kornhauser [5] in 1990. Since then, a large amount of 1-D models have been developed on this basis. The computations are performed in only one direction along the flow inside the ejector. Even more streamlined, zero-dimension-models consider only the inlet and outlet parameters of the ejector. The calculation of thermodynamic parameters is most widely based on the steady state in the two-phase-ejector modeling observed in the literature [8–10, 14]. The main advantage of zero/one-dimension-models is the ability to rapidly generate results [16].

The modeling method also varies according to the state of the fluid. The homogeneous relaxation model (HRM) and delayed equilibrium model (DEM) are based on a non-thermodynamic equilibrium state, while the homogeneous equilibrium model (HEM) is based on the thermodynamic equilibrium state for the entire two-phase region. HRM approach assumes that at high Reynolds and Weber numbers, the scales at which turbulent mixing occurs are separate from those of the bulk fluid motion, allowing the turbulent mixing and generation of interfacial surface area to be resolved through classical turbulence closures. Relatively, the DEM method introduces an additional fraction of the metastable liquid that is gradually submitted to isentropic flashing. Table 1 provides a summary and overview of part of the research on the ejector modeling from various scholars.

In addition to the modelings of ejectors, many researchers have conducted experimental studies on ejectors to quantify their performance in a heat pump cycle. Parametric analysis has been performed to obtain the operation pattern of ejectors in the system at different pressure and temperature levels, and to study the performance variation of ejectors with different geometrical dimensions [16, 18, 22–27]. Table 2 provides a

Table 1: Summary of the research studies on modeling of the pressure recovery ejector implanted in a heat pump and refrigeration cycle

Author	**Model**	**Remarks**
Jahar Sarkar [8]	1-D HEM	Second law efficiency can be improved by maximum 9 %.
Deng et al. [9]	1-D HEM	The ejector improves the maximum COP by up to 18.6 % compared to the internal heat exchanger system and by 22.0 % compared to the conventional system.
Ameur et al. [15]	1-D HEM	Pressure recovery took place in the mixing section and the diffuser. Vapor quality increases mainly at the outlet of the primary nozzle where the liquid is expanded to very low pressure.
Li and Groll [17]	1-D HEM	The COP of the ejector expansion transcritical CO2 cycle can be improved by more than 16 % over the basic transcritical cycle for typical air conditioning operation conditions.
Liu et al. [18, 22]	1-D HEM	A method of determining the efficiencies of ejector motive nozzle, suction nozzle, and mixing section based on the measured performance data was developed. However, this method has not been widely used due to the constraints on the operation parameters.
Banasiak and Hafiner [16, 20]	1-D DEM	Delayed Equilibrium Model supplied with the Homogeneous Nucleation Theory for the purpose of the metastable states analysis for a transcritical flow with delayed flashing over the motive nozzle. The absolute values of the relative simulation errors for both the overall pressure lift (2.66 % on average) and the critical mass flow rate (1.84 % on average) were acceptably low.
Lucas et al. [12]	CFD HEM	The numerical simulation predicted the experimentally determined driving mass flux within an error range of 10 %, and the maximal derivation of pressure recovery is up to 20 %.
Smolka et al. [14]	CFD HEM	The numerical results showed good agreement with the measured values. The model was developed in 3-D geometry and showed some non-symmetries in the obtained results, which are contrary to most of the axisymmetric models in the literature.
Colarossi et al. [13]	CFD HRM	The occurrence location of pressure recovery is affected by the motive and suction inlet velocity as well as the ejector geometry. The flow is near thermodynamic equilibrium in the diffuser. Turbulent viscosity is greatest in the mixing section.

summary and overview of part of the research on the experimental study from various scholars.

Concluded from current literature, zero/one-dimension-models based on thermodynamic equilibrium state

Table 2: Experimental research studies for ejectors in the field of heat pump and refrigeration cycles

Author	**Research Domain**	**Remarks**
Banasiak et al. [16]	Ejector design	Different ejector configurations were examined, including various lengths and diameters of the mixer and various angles of divergence for the diffuser.
Liu et al. [18, 22]	Ejector design	Empirical correlations were established to estimate ejector component efficiencies at different ejector geometries and operating conditions.
Chunnanond and Aphornratana [23]	Parametric analysis, Ejector design	An experimental steam ejector refrigerator was constructed to examine the influences of the operating conditions, the superheated level of the primary fluid, and the geometry, including the position of the primary nozzle, on the system performance.
Zhu et al. [24]	Parametric analysis	The ejector performance of the entrainment ratio, pressure lift ratio, and efficiency were investigated under various primary flow pressure, secondary flow pressure, and back pressure conditions.
Nakagawa et al. [25]	Ejector design	The effect of mixing length on ejector system performance was analyzed experimentally. The mixing lengths used were 5 mm, 15 mm, and 25 mm, with constant rectangular cross-section.
Aligolzadeh and Fard [26]	Ejector design	A practical methodology is presented to and provides a road map to design a multi-ejector refrigeration system with maximum seasonal COP that provides the required cooling load of a building over a hot season.
Haberschill et al. [27]	Ejector design	The experiments investigated the variation of ejector geometry such as the motive nozzle throat diameter, the mixing chamber diameter and the distance between the motive nozzle and the diffuser on the ejector working characteristics and the system performance.

are by far the most studied models. However, the accuracy of the zero/one-dimensional model in predicting the ejector outlet pressure, the entrainment ration, and other parameters for various operating conditions needs to be verified with further experimental data. The effect of the simplification during zero/one-dimension modeling is also unclear. Moreover, few studies have been devoted to the comparative analysis of different zero/one-dimension-models. This paper compares two typical 1-D HEM models which are representative of the

existing models available in the literature [9, 17]. Experimental data from Zhu et al. [24] and Haberschill et al. [27] are used to validate and compare the two models. By comparing and analyzing the discrepancies between experimental data and simulation results, the source of deviation is diagnosed and corrected. Quantitative analysis is performed on the prediction accuracy of the two selected typical 1-D ejector models implanted in CO_2 transcritical cycle. The present research work can provide a guideline for the subsequent optimization of 1-D ejector numerical simulation.

2. Experimental data

Two sets of independent experimental data compiled from the current literature are used to compare and validate the models [24, 27]. By comparing the simulation results with the experimental data under the same operating parameters, the accuracy of the two models can be analyzed and compared.

2.1. Experimental setup from Zhu et al. [24]

The first group of experimental data obtained from Zhu et al. [24] is briefly described here. The schematic of this experimental rig is shown in Fig. 3. In the ejector expansion refrigeration cycle, the compressor used is DORIN CD180H with a 7.5 kW inverter to control the compressor speed. The gas cooler is a counter-flow plate heat exchanger rated at 7.5 kW with water as the coolant. The evaporator has a parallel flow microchannel heat exchanger with a variable speed fan to control the superheat of the evaporator outflow. And the capacity of the evaporator is 5 kW. In addition, a fan heater with a maximum capacity of 3 kW is placed near the evaporator to maintain room temperature.

The range of the input pressure and temperature values as well as the mass flow rates for the motive and suction flows are listed in Table 3.

Table 3: Range and measurement accuracy of the input parameters, data from Zhu et al. [24]

	Mass flow rate ($\dot{m}_m/\dot{m}_s$)	Input pressures (P_m/P_s)	Input temperatures (T_m/T_s)
Range	60.0 to 109.5 / 13.3 to 65.1 kg/h	8.1 to 9.9 / 2.98 to 3.67 MPa	34.9 to 35.8 / 20.5 to 24 °C
Accuracy	± 0.1 %	± 0.1 %	± 0.2 °C

2.2. Experimental setup from Harberschill et al. [27]

To further validate the accuracy of the models, an additional group of experimental data is taken from a prototype of an air/water refrigeration machine using CO_2 as a refrigerant [27]. The simplified cycle schematic is shown in Fig. 4. The system is composed of three circuits that are independent of each other. The first one is the CO_2 circuit. The second one is an auxiliary water circuit whose temperature and flow rate are controlled to simulate the variation of the hot source. The third one is an air circuit, regulated in temperature and humidity to simulate the variations of the climatic conditions. A Bock RKX26/31-4 brand 6-cylinder semi-hermetic radial piston compressor is powered by a Danfoss variable speed driver and operates from 0 to 1450 rpm. A coaxial high-pressure water exchanger is installed to cool the vapor.

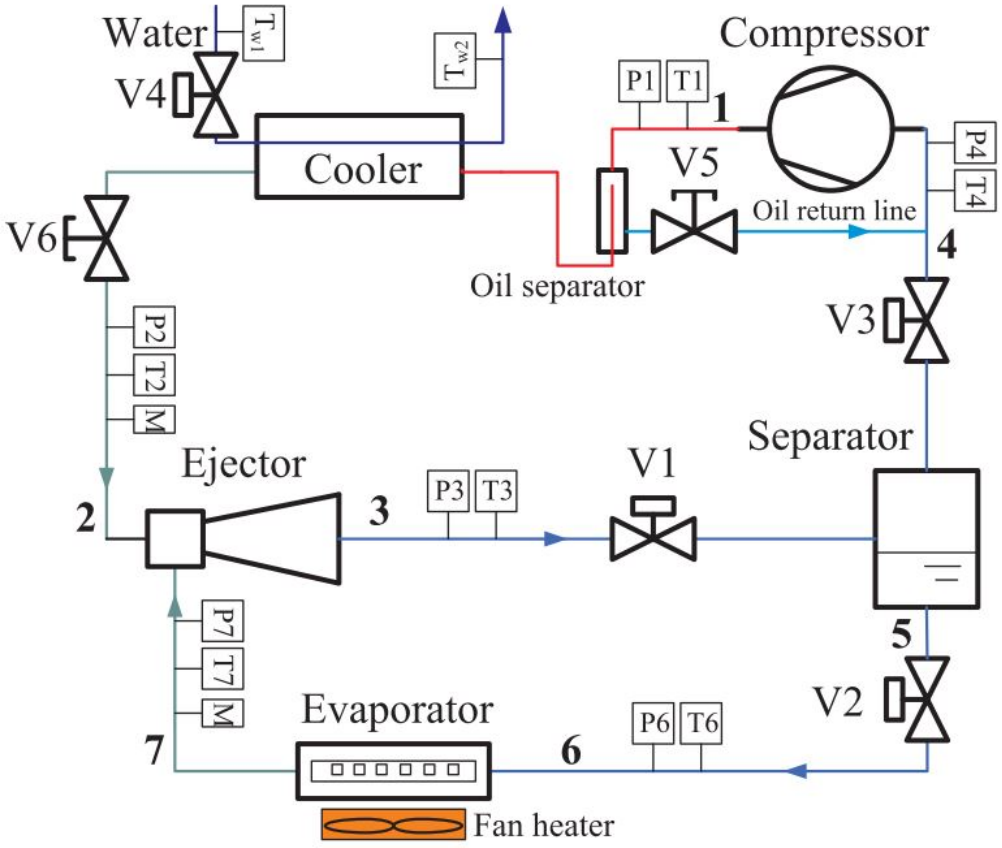

Figure 3: Schematic of the test bench from Zhu et al. [24]

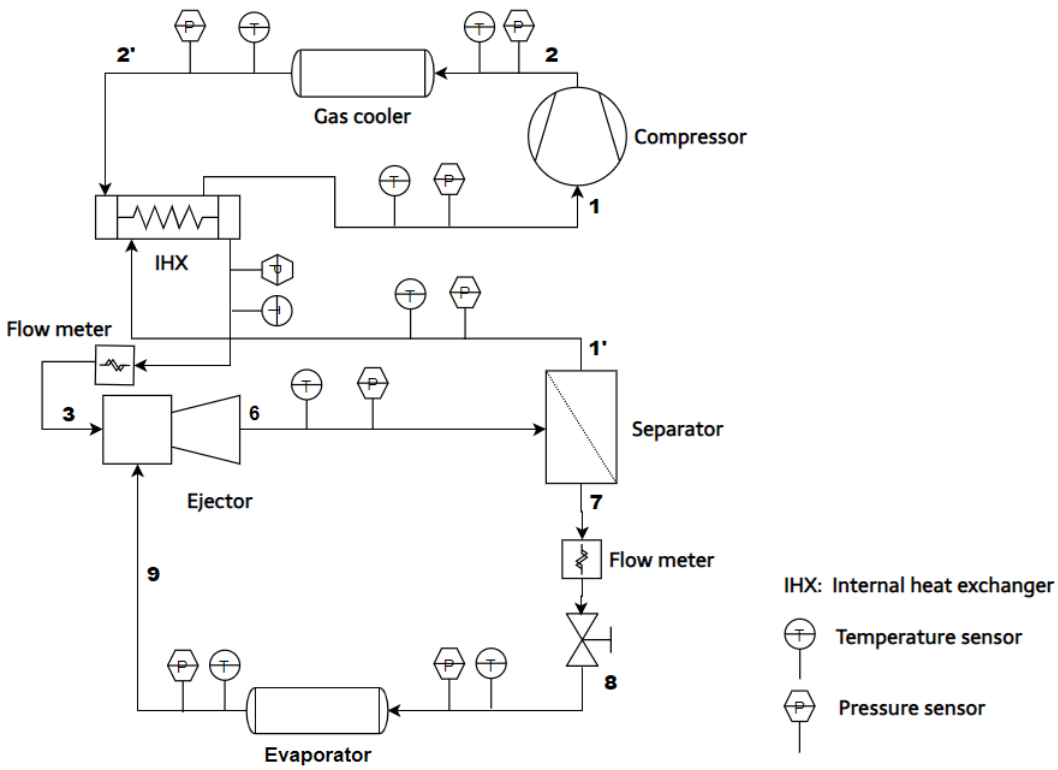

Figure 4: Schematic of the test bench from Harberschill et al. [27]

From Fig. 4, an internal heat exchanger is installed in the system, which allows the supercritical flow at high temperature from the gas cooler to preheat the saturated vapor exiting from the separator. As an adjustment to the model, the temperature of heated vapor is taken as an additional input, and the outlet parameters of the cooled fluid are calculated according to the energy balance. The range of the input pressure and temperature values as well as the mass flow rates for the motive and suction flows are listed in Table 4.

Table 4: Range and measurement accuracy of the input parameters, data from Harberschill et al. [27]

	Mass flow rate ($\dot{m}_m/\dot{m}_s$)	Input pressures (P_m/P_s)	Input temperatures (T_m/T_s)
Range	139.7 to 185.3 / 36.4 to 62.8 kg/h	7.8 to 10.3 / 2.2 to 3.0 MPa	33.5 to 52.1 / -9.5 to 4.3 °C
Accuracy	0.5 %	± 0.5 %	± 0.5 °C

3. Modeling/methodology

The 1-D HEM models are classified into two categories based on the variation of pressure before and after the mixing process inside the ejector: the first group neglects the pressure variation during the mixing process and for the second group the pressure variation is considered. Two 1-D HEM models [9, 17] that represent the above categories are selected to study two-phase flow in the ejector which is implanted in a transcritical

CO_2 heat pump cycle. In this paper, the two groups of models are named as constant pressure mixing model [9] and variable pressure mixing model [17].

3.1. Modeling of the ejector of the variable pressure mixing model [17]

For variable pressure mixing model, the simulation is based on the system schematic shown in Fig. 1 and is referred to Li and Groll [17]. As explained in the original article, some assumptions are applied to simplify the simulation [17]:

1. Pressure drop along the pipe and in the main components is neglected.
2. The system is adiabatic except for heat exchange with the environment in the gas cooler and evaporator.
3. Kinetic energies of the refrigerant at the ejector inlet and outlet are negligible.
4. The flow through the throttle valve is isenthalpic.
5. The friction losses in the mixing section is neglected.

According to above assumptions, the modeling proceeds sequentially by components in the system. Inside the ejector, the motive stream is accelerated with a pressure drop from P_3 to P_4 before mixing. P_4 is slightly lower than the evaporation pressure P_9. The pressure difference between state 4 and state 9 is supposed to vary with the operating parameters. Li and Groll [17] investigated the effect of various pressure differences (0.01 MPa, 0.03 MPa and 0.05 MPa) on the ejector entrainment ratio and system COP, but no correlation was provided. Moreover, there is no available methodology in the open literature to calculate the pressure difference. Therefore, 0.03 MPa is set as the default value in the variable pressure mixing model.

The enthalpy of the motive flow at the outlet of the nozzle is determined by Eq. 2, where η_m is the isentropic efficiency of the motive nozzle and $h_{m,is}$ is the ideal enthalpy for an isentropic expansion. The flow velocity of the motive flow (u_m) at the nozzle outlet can be obtained by an energy balance between states 3 and 4 using Eq. 3, where $h_{4,m}$ is the enthalpy of the motive flow at the nozzle outlet. The density of the motive flow at the nozzle outlet can be found with a property relationship by Eq. 4.

$$h_{4,m} = h_3 - \eta_m \cdot (h_3 - h_{m,is}) \tag{2}$$

$$\frac{1}{2} \cdot {u_m}^2 = h_3 - h_{4,m} \tag{3}$$

$$\rho_m = f(h_{4,m}, P_4) \tag{4}$$

Using the conservation of mass, the area occupied by the motive flow at the nozzle outlet per unit total ejector flow rate is given by Eq. 5, where w is the entrainment ratio of ejector.

$$a_m = \frac{1}{(1+w) \cdot \rho_m \cdot u_m} \tag{5}$$

The suction flow also slightly expands in the suction nozzle and the calculation of the outlet enthalpy and the flow velocity is analogous to the motive flow, given by Eq. 6 to Eq. 9.

$$h_{4,s} = h_9 - \eta_s \cdot (h_9 - h_{s,is}) \tag{6}$$

$$\frac{1}{2} \cdot {u_s}^2 = h_9 - h_{4,s} \tag{7}$$

$$\rho_s = f(h_{4,s}, P_4) \tag{8}$$

$$a_s = \frac{w}{(1+w) \cdot \rho_s \cdot u_s} \tag{9}$$

For the mixing process, an unknown pressure P_{mix} will be introduced. According to the conservation of momentum before and after the mixing of the motive and suction flows, Eq. 10 is obtained, where u_{mix} is the flow velocity of the mixed flow. According to the conservation of energy, the enthalpy of the fluid after the mixing can be obtained by Eq. 11.

$$P_4 \cdot (a_m + a_s) + 1/(1+w) \cdot u_m + w/(1+w) \cdot u_s = P_{mix} \cdot (a_m + a_s) + u_{mix} \tag{10}$$

$$(1+w) \cdot (h_{mix} + \frac{1}{2} \cdot {u_{mix}}^2) = h_{4,m} + w \cdot h_{4,s} \tag{11}$$

An isentropic efficiency η_d is assumed to determine the isentropic outlet enthalpy of ejector (Eq. 12). The ejector outlet enthalpy h_6 is obtained by the energy balance between the inlet and the outlet of the ejector (Eq. 13). Then the outlet pressure is acquired by state equations with the known outlet enthalpy and the entropy for an isentropic process.

$$h_{6,is} = \eta_d \cdot h_6 + (1 - \eta_d) \cdot h_{mix} \tag{12}$$

$$h_6 = 1/(1+w) \cdot h_3 + w/(1+w) \cdot h_9 \tag{13}$$

After obtaining the ejector outlet pressure, along with the calculated actual enthalpy at the outlet, more thermodynamic parameters, such as entropy and vapor quality, can be acquired through the state equations. To this point the modeling of the ejector is terminated.

3.2. modeling of the ejector of the constant pressure mixing model [9]

For the constant pressure mixing model, common assumptions with the variable pressure mixing model in section 2.1 are applied during the simulation, and the modeling process refers to Deng et al. [9]. In contrast to the variable mixing pressure model, the suction flow is not expanded in the nozzle, and the motive flow expands to the evaporation pressure at the nozzle outlet (Eq. 14). The most significant difference between the two models is that the pressure does not change before and after the mixing of the motive and suction flows. The velocity of the mixed flow is computed by the momentum balance (Eq. 15). Except for these differences,

the simulations of the ejector nozzle and the diffuser are identical to the variable pressure mixing model (Eq. 2 and Eq. 3, Eq. 12 and Eq. 13 respectively), without duplicate description in this section.

$$P_4 = P_9 \tag{14}$$

$$u_m/(1+w) = u_{mix} \tag{15}$$

3.3. Modeling of other components

After expansion in the ejector, the mixed flow goes through the separator where the saturated vapor is compressed in the compressor and the saturated liquid expands through the valve and enters into the evaporator. In this section, the modelings of different components in the system are introduced in sequence referring to the literature by [9, 17].

For the modeling of the compressor, the compression is assumed as adiabatic and an isentropic efficiency η_{comp} is introduced to characterize the performance of the compressor. With the isentropic efficiency and a fixed outlet pressure of the compressor, the outlet enthalpy can be calculated by Eq. 16, where h_1 and $h_{2,is}$ are the inlet enthalpy and outlet enthalpy of an isentropic process for the compressor. The other thermodynamic parameters can be obtained by the state equations. The power consumed by the compressor can be expressed by Eq. 17, where $\dot{m}_m$ is the mass flow rate of the motive flow.

$$\eta_{comp} = \frac{h_{2,is} - h_1}{h_2 - h_1} \tag{16}$$

$$\dot{W}_{comp} = \dot{m}_m \cdot (h_2 - h_1) \tag{17}$$

Compressed in the compressor, the motive flow is then cooled in the gas cooler. The outlet pressure and temperature are known during modeling. The outlet enthalpy is also known with state equations. With inlet and outlet enthalpies, the capacity of the gas cooler is calculated using Eq. 18.

$$\dot{Q}_{heating} = \dot{m}_m \cdot (h_2 - h_3) \tag{18}$$

After exiting the separator, the saturated liquid flows through a throttle valve and is heated to the saturated or superheated vapor in the evaporator. The expansion through the valve is considered isenthalpic in the modeling ($h_8 = h_7$). Then the cooling capacity of the evaporator is expressed by Eq. 19, where h_9 is known with input values of the temperature and the pressure.

$$\dot{Q}_{cooling} = \dot{m}_s \cdot (h_9 - h_8) \tag{19}$$

In the referenced literature [9, 17], the heat pump is used for cooling application, so the COP of cooling is selected as the system evaluation indicator and is calculated by Eq. 20.

$$COP_{cooling} = \frac{\dot{Q}_{cooling}}{\dot{W}_{comp}} \tag{20}$$

3.4. Resolution of the numerical models

Based on the original reference [9, 17] and following the basic modeling framework as described in the former sections, the realization and operation of the models are completed using Matlab. The flow charts of the modeling process of the ejector for the two models are depicted as in Fig. 5. All the thermodynamic parameters are acquired through the Python package of the Coolprop integrated in Matlab.

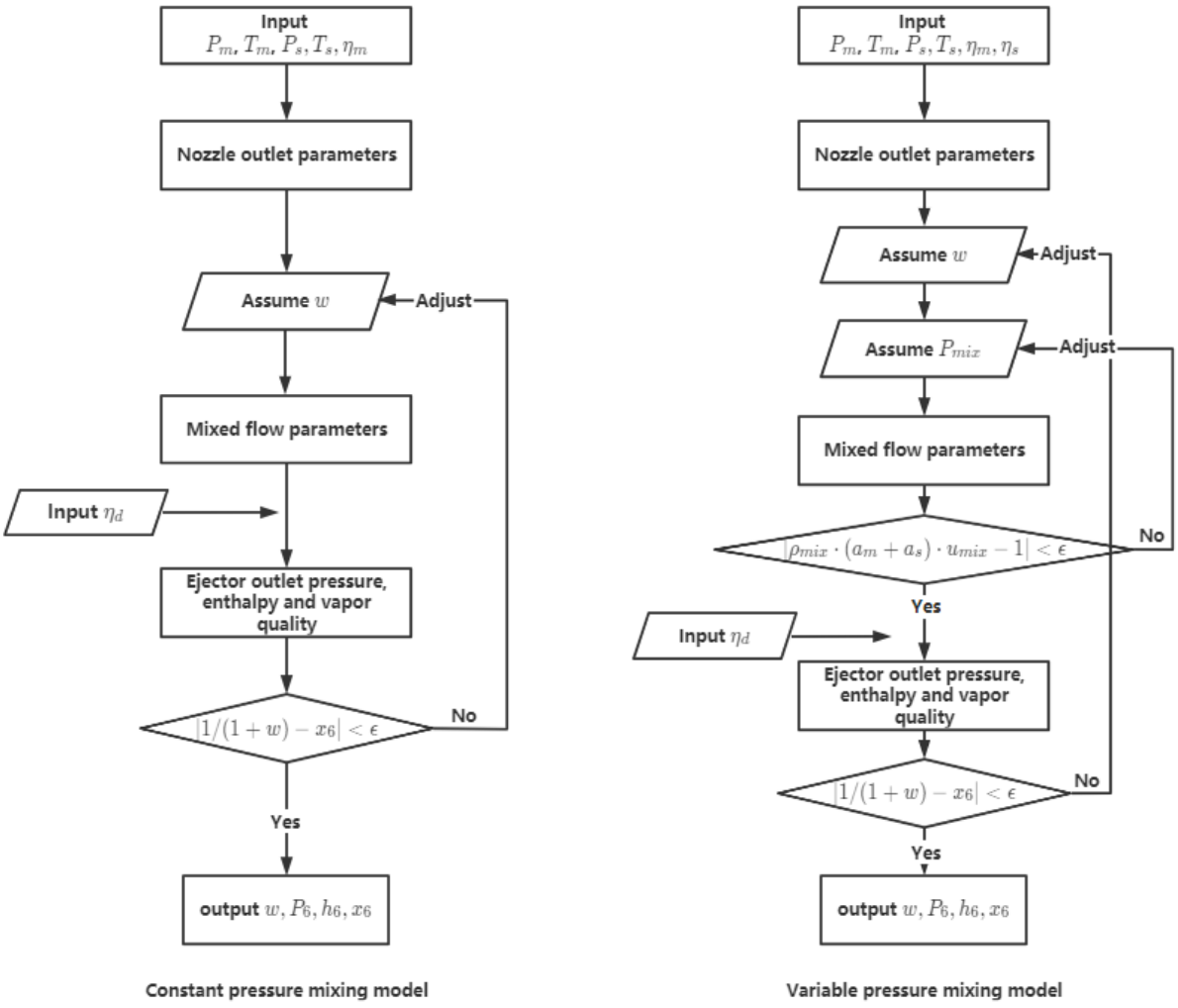

Figure 5: Flow chart of modeling sequence for the ejector models

For the two models, the input parameters include the temperature and pressure values at the ejector inlets, as well as the isentropic efficiencies of the ejector components and the compressor. Since the friction losses in the mixing section are not accounted in both models, the mixing efficiency of the ejector is assumed as 1 rather than an input parameter. Liu et al. [18] established an empirical correlations to estimate the ejector component efficiencies at different ejector geometries and operating conditions. However, these correlations should be used within the following boundaries:

1. 8.0 MPa $< P_m <$ 14.0 MPa, 2.5 MPa $< P_s <$ 5.0 MPa;
2. 40 °C $< T_m <$ 60 °C, 15 °C $< T_s <$ 26 °C;

3. 0.1 g/s $<\dot{m}_m<$.25 g/s, 0.05 g/s $<\dot{m}_s<$ 0.07 g/s;

4. 1.8 mm $<D_t<$ 2.7 mm, $D_{mix} = 4$ mm;

It is clear that the correlation applies to more restrictive conditions, and neither of the two sets of data cited in this paper [24, 27] matches this condition. Therefore, the geometries of the ejector are not used as input parameters during the simulation, instead, like most similar models, the isentropic efficiencies of the ejector components are fixed to the appropriate values. The input isentropic efficiencies of the ejector nozzle and the diffuser are set as 0.6 for the tested ejector from Haberschill et al. [27] due to the generally inferior performance. For the ejector of Zhu et al. [24], 0.8 is selected as the default isentropic efficiency for the ejector components owing to the better performance based on the analysis of the experimental data.

The closure of the simulation is based on the tolerated deviation (ϵ) of the iterated parameters. In the constant pressure mixing model, there is only one unknown parameter: entrainment ratio w which needs to be found by an iteration based on the mass balance of the vapor between the inlet and the outlet of the ejector, as depicted by Eq. 21, where x_6 is the vapor quality at the ejector outlet which is acquired by the state equations.

$$x_6 = 1/(1 + w) \tag{21}$$

In the variable pressure mixing model, besides entrainment ratio, the pressure value after the mixing of the motive and suction flows is also unknown and needs to be found by an iteration. The closure criteria is the mass conservation of the mixed flow (Eq. 22), where ρ_{mix} is the density of the mixed flow.

$$\rho_{mix} \cdot (a_m + a_s) \cdot u_{mix} = 1 \tag{22}$$

The output parameters of the ejector modeling are the pressure and enthalpy values at the entrance and the exit of each section, the outlet vapor quality and the entrainment ratio of the ejector. After obtaining these parameters, and running the models for the remaining components as described in the above section, the modeling of the ejector expansion heat pump cycle is terminated.

After reproduction of the two models based on the original works [9, 17], the simulated entrainment ratio, ejector outlet vapor quality, COP and relative performance ratio are compared with the original simulation values from the respective articles [9, 17], and they show a good agreement as depicted in the appendix. As a result, the models are validated and can be used to compare with each other using the independent experimental data, which has never been done in the literature before.

3.5. Liquid mass balance in the separator

For the ejector expansion cycle, the motive flow is mixed with the suction flow and exits the ejector in a two-phase flow. In the separator, the liquid at the ejector outlet is separated and flows to the evaporator. On the contrary, the vapor from the ejector outlet is split and enters the compressor, as shown in Fig. 6. When the system operates steadily, there is a general mass balance for the separator defined by Eq. 23 that is satisfied. In parallel, the liquid mass balance is defined by Eq. 24. Under this equilibrium, the liquid level

in the separator is constant and the liquid portion of the ejector outlet flow is completely separated by the separator and flows to the evaporator. Both the 1-D models studied are based on such a steady state.

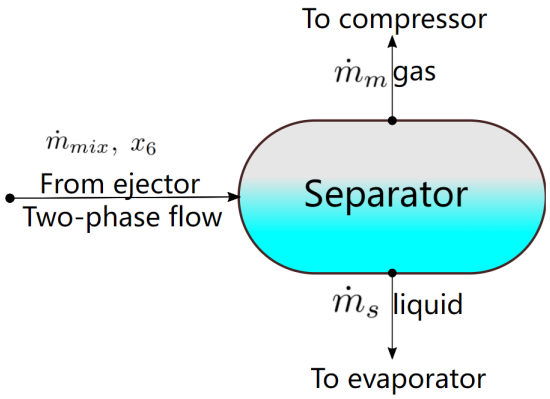

Figure 6: Liquid mass balance before and after the separator

$$\dot{m}_{mix} = \dot{m}_m + \dot{m}_s \tag{23}$$

$$\dot{m}_{mix} \cdot (1 - x_6) = \dot{m}_s \tag{24}$$

However, it is known from the computations based on the two sets of experimental data [24, 27] that the equilibrium is hardly maintained in the actual system operation for the most cases. Meanwhile, when the actual system operates at steady state under the specific working conditions (e.g. temperature, pressure, compressor speed, capacity of the gas cooler and evaporator), it is observed that the liquid level in the separator continuously changes (rises or falls). The operating state of the actual system is named as pseudo-steady state to distinguish from the steady state in the 1-D models. The general mass balance for the separator is still valid under the pseudo-steady state but the liquid balance (Eq. 24) before and after the separator is broken and the liquid level constantly changes during the operation. As a matter of fact, a larger volume of separator is used for the experimental test facility to avoid being completely filled with vapor or liquid and to guarantee a stable operation period [24, 27].

The liquid imbalance is mainly caused by the mismatch between the entrainment ratio of the ejector and the vapor quality at the ejector outlet. That is, in the actual operation, for a selected ejector, the entrainment ratio w and vapor quality x_6 will satisfy Eq. 21 (equivalent to Eq. 24) only under specific operating condition which is hard to maintain and predict. However, for the actual operating system, Eq. 21 does not always hold because the operating parameters such as pressures and temperatures will deviate from the specific value for steady state and the system lacks self-regulation, so the liquid level in the separator is also dynamically changing. That's why some scholars have proposed improved ejector refrigeration systems to control the liquid level of the separator [8, 10, 17].

A new expression of the coefficient of liquid mass balance [24] for the vapor-liquid separator, β, is defined

by Eq. 25. β can be used to quantify the deviation of the separator between the pseudo-steady state during the actual operation and the steady state.

$$\beta = (\dot{m}_{mix} \cdot (1 - x_6) - \dot{m}_s)/\dot{m}_s \tag{25}$$

The imbalance represents the existence of excess vapor or liquid at the outlet of the separator due to the performance limitation of the separator (the vapor and liquid can not be perfectly separated). When β is negative, it indicates that the there is surplus liquid at the separator outlet. In contrast, when β is positive, it means there is an excess vapor at the outlet.

The two 1-D HEM models studied in our paper are derived from the literature, which are widely used by many scholars. Since the models studied are in a different operating state from the actual experimental test systems [24, 27], and since there are currently no scholars who have built an actual experimental system with liquid level regulation control device. In order to validate the 1-D HEM models using the available experimental data [24, 27] and based on steady state (without liquid imbalance), a data post-processing method based on a hypothetical system is introduced (inspired by the new configuration of the ejector expansion refrigeration system from He et al. [10]). The schematic of the hypothetical corrected system is depicted as Fig. 7. The method is not a restructuring of the actual operating system, but to extrapolate the system performances if it operated without liquid imbalance. Then the proceeded experimental data can be used to validate the two 1-D numerical models that operate at steady state without the liquid imbalance.

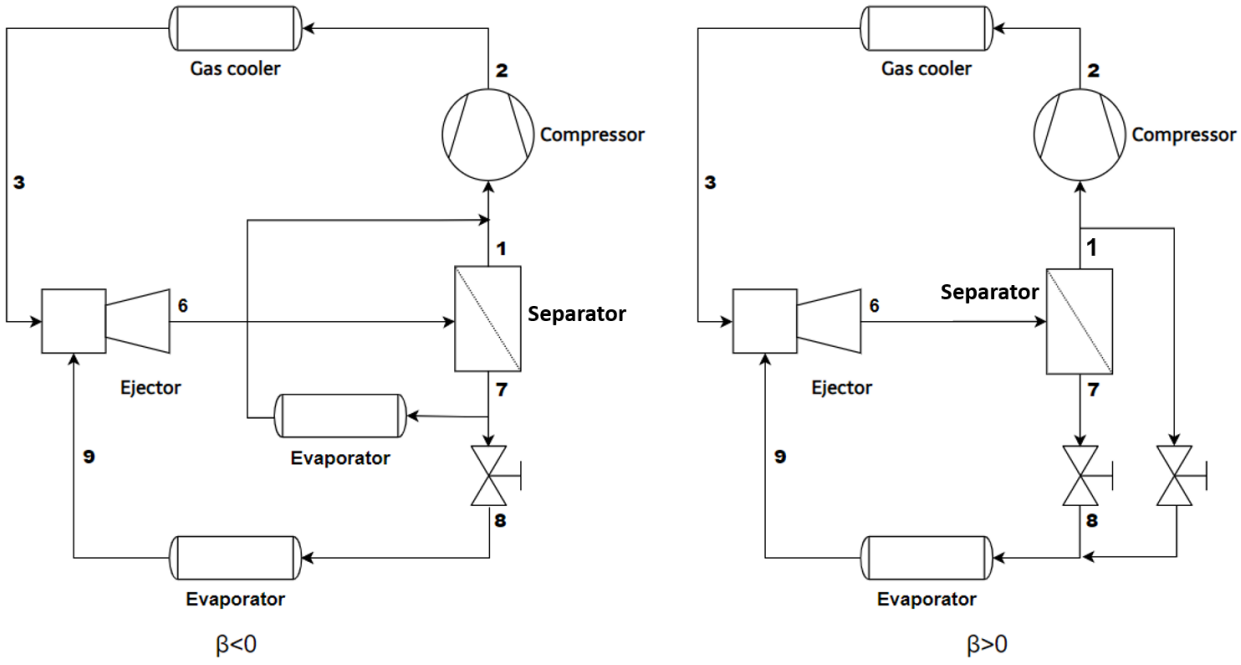

Figure 7: Schematic of the hypothetical optimized system for the data post-processing. β is the liquid balance rate (Eq. 25)

From Fig. 7, there are two cases for data processing based on the value of β. To offset the excess liquid (β is negative), it can be assumed that an additional evaporator is installed to evaporates the liquid into

saturated vapor. The saturated vapor mixes with the vapor from the separator outlet and then flows into the compressor. For the case of excess vapor at the outlet (β is positive). It can be assumed that there is a bypass loop to mix the excess vapor at the outlet of the separator with the two-phase flow exiting after the expansion valve. The mixture then enters into the evaporator.

The mass flow rates of the motive and suction flows after data post-processing are determined by the vapor quality at the ejector outlet. The unit mass flow rate of motive and suction flows can be expressed by Eq. 26 and Eq. 27, where w_{new} is the new entrainment ratio after data post-processing. The unit mass flow rate is based on the basis that the total flow rate is 1.

$$\dot{m}_{p,unit} = 1/(1 + w_{new}) = x_6 \tag{26}$$

$$\dot{m}_{s,unit} = w_{new}/(1 + w_{new}) = 1 - x_6 \tag{27}$$

After data post-processing, for the compressor, the inlet and outlet temperatures and pressures are unchanged, so the variation of compression work is only related to the correction of the mass flow rate.

The capacity of the evaporator will change accordingly to the value of β. When β is negative, besides the change due to the mass flow rate correction, the capacity of the extra evaporator has to be considered. The modified capacity of the evaporator for unit total mass flow rate is calculated using Eq. 28 and Eq. 29. Where $\dot{m}_{s,unit} \cdot \beta$ is the mass flow rate in the extra evaporator and $h_1 - h_7$ is the enthalpy change.

$$\dot{Q}_{cool,extra,unit} = \dot{m}_{s,unit} \cdot \beta \cdot (h_1 - h_7) \tag{28}$$

$$\dot{Q}_{cool,unit} = \dot{m}_{s,unit} \cdot (h_9 - h_8) + \dot{Q}_{cool,extra,unit} \tag{29}$$

When β is positive, in addition to the correction of the flow rate, the enthalpy of the inlet also changes due to the mixing of the two fluids at the inlet. The new capacity of the evaporator for unit total mass flow rate is calculated by Eq. 30 and Eq. 31, where $h_{8,new}$ is enthalpy value of mixed fluid at state 8.

$$h_{8,new} = (\dot{m}_s \cdot h_8 + \dot{m}_s \cdot \beta \cdot h_1)/((\dot{m}_m + \dot{m}_s) \cdot (1 - x_6)) \tag{30}$$

$$\dot{Q}_{cool,unit} = \dot{m}_{s,unit} \cdot (h_9 - h_{8,new}) \tag{31}$$

With such recalculation applied to the obtained experimental data, the liquid imbalance during the operation of the actual system can be eliminated, then the corrected experimental data allows to validate the models under a steady state.

4. Results and discussion

4.1. Sensitivity analysis for input isentropic efficiencies of ejector components and compressor

The efficiencies of the ejector components depend on various factors such as the ejector geometry, the flow path design, the working fluid, as well as the pressure and temperature values. In most of the studied literature, values ranging from 0.5 to 0.95 are assumed for the individual ejector component isentropic efficiencies [22]. To investigate the impact of these efficiencies on the overall numerical 1-D model, this section presents a sensitivity analysis of the isentropic efficiencies of the ejector components and the compressor using the reproduced 1-D models. During the sensitivity analysis, for both models the cycle operates at identical working conditions as shown in Table 5.

Table 5: Input parameters for sensitivity analysis

Gas cooling pressure	Evaporation pressure	Gas cooler outlet temperature	Evaporation temperature
101.27 bar	25.40 bar	48.05 °C	0.29 °C

The results of the sensitivity analysis of the constant pressure mixing model are shown in Fig. 8. The default efficiencies for the nozzle, the diffuser and the compressor are 0.8, 0.8 and 0.75 respectively. From the Fig. 8, the cycle COP increases as the efficiency of the component improves, and the correlation is nearly linear. Among the three component efficiencies, the COP is most sensitive to the efficiency of the compressor. When the isentropic efficiency of the compressor increases from 0.3 to 0.9, the COP rises from 0.47 to 1.49. The relative change in COP is around 200 %. For the motive nozzle and the diffuser, the two curves almost overlap, which indicates that the isentropic efficiency of the motive nozzle and the diffuser has almost the same effect on the system COP in this model. The sensitivity related to motive nozzle and the diffuser is much lower than the compressor, and the relative change in COP is nearly 36 %.

For the variable pressure mixing model, since the model considers that the suction flow also slightly expands in the nozzle, an extra efficiency is added in the analysis. Same as the model above, the variation interval of component efficiencies is between 0.3 and 0.9. The default efficiencies for the motive nozzle, suction nozzle, diffuser and compressor are 0.9, 0.9, 0.8 and 0.75 respectively. The trend of COP with the change of each component efficiency is shown in Fig. 9. From Fig. 9 we can conclude that the isentropic efficiency of the compressor has the most significant impact on the system COP and is much greater than the individual components of the ejector. Among the ejector components, system COP is more sensitive to the motive nozzle efficiency, next is the suction nozzle and the last is the isentropic efficiency of the diffuser. Specifically, when the isentropic efficiency of each component increases from 0.3 to 0.9, the corresponding relative changes in COP are 200%, 18%, 10% and 3% respectively.

From the above analysis, it is clear that the COP of the system is more sensitive to the isentropic efficiency of the compressor than that of the individual components of the ejector. Therefore, when conducting 1-D simulations of the ejector expansion cycle, it is necessary to verify the deviation of the input efficiency of the compressor to avoid the simulation failure. However, for the compressor, the approximate performance curves

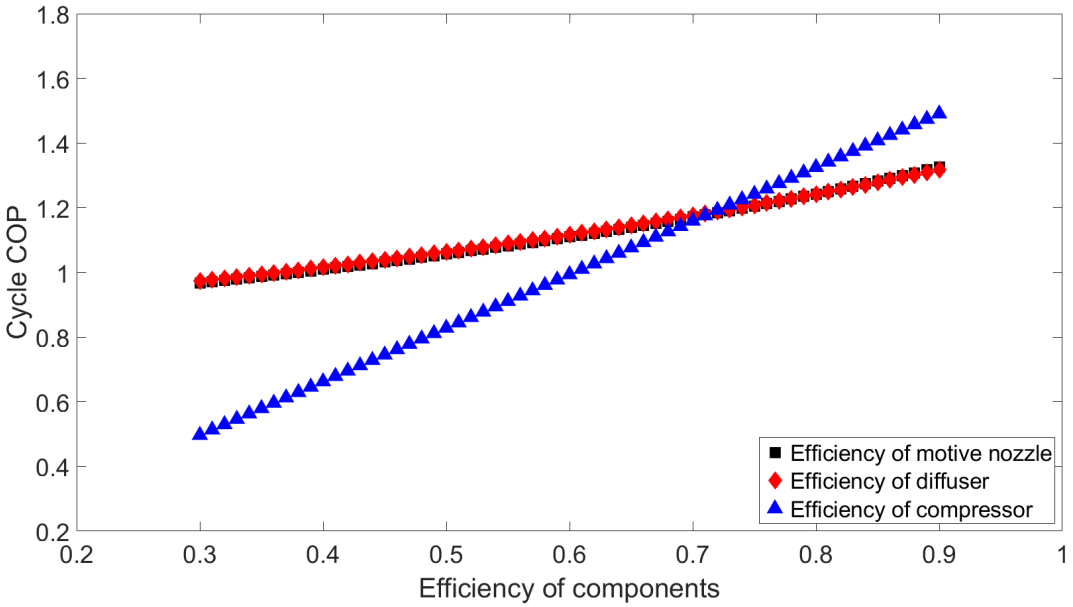

Figure 8: Sensitivity analysis for the ejector components and compressor efficiencies, constant pressure mixing model [9]

provided by the manufacturers often serve as a reference during simulations. But for the ejector components, there is no accurate and applicable calculation formula in the available literature. Therefore, deviations of ejector component's efficiencies in the modeling process can also lead to large cumulative simulation errors.

4.2. Experimental validation and comparative analysis of 1-D models

To validate the 1-D models studied in this paper, the necessary input parameters are the input temperatures and pressures of the motive and suction flows. When using the data set from Haberschill et al. [27], the outlet temperature of the internal heat exchanger for the heated flow is taken as an extra input parameter. Considering the significant impact on the system performance, the compressor efficiencies of both test units are obtained from the corresponding experimental data in order to avoid large deviations.

The two 1-D models are verified with the two selected groups of independent experimental data, the performance indicator for the test facility is the COP for refrigeration applications. For both models, the simulated entrainment ratio of the ejector is compared to the value derived from the measured flow rate of the primary and suction flows. Other parameters such as the outlet pressure and vapor quality of the ejector are also verified with the experimental data.

The validation of the two 1-D models is conducted in two groups, the first group is validated with the original experimental data, while the second group is verified with the processed experimental data, when the liquid imbalance of the system is eliminated. Fig. 10 to Fig. 13 describe the deviation of the simulation results of both models on the COP and entrainment ratio. In a comprehensive comparison, the deviation distribution of the two models are similar. Before data post-processing, the relative errors of the COP and entrainment ratio vary from nearly 0 to more than 50 % for both models. This indicates that neither model can predict accurately enough on the cycle performance nor the operation of the ejector for most cases. For the data from

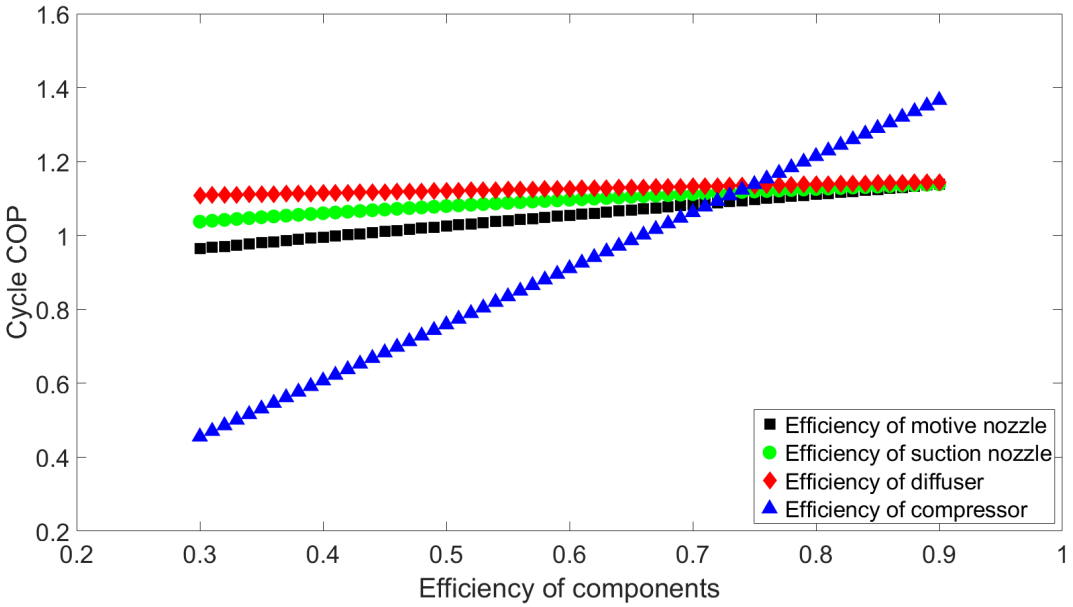

Figure 9: Sensitivity analysis for the ejector components and compressor efficiencies, variable pressure mixing model [17]

Zhu et al. [24], there is better agreement between the simulated and experimental values for the COP, but the deviation could still reach 30%. This indicates that due to the effect of the liquid imbalance before and after the separator, both 1-D models are not accurate for the COP and entrainment ratio prediction.

After post-processing of the experimental data to eliminate the effects of liquid imbalance, the relative deviations of the COP and entrainment ratio are significantly reduced. Specifically, the deviation of COP is reduced from 30% to 15% using the data from Zhu et al. [24] as a reference. And for the experimental data of Haberschill et al. [27], the deviation is also reduced from 50% to about 15%. For the entrainment ratio, the discrepancy is almost eliminated, with the relative deviation less than 5%.

To quantitatively compare the accuracy of the two models, average deviation and variance value are introduced. For the data set of Zhu et al. [24], the average absolute deviation of the COP and entrainment ratio is 13.14 % and 1.35 % accordingly for the constant pressure mixing model. For the variable pressure mixing model, the corresponding values are 10.71 % for the COP and 1.58 % for the entrainment ratio. For both models, the variance of these parameters is almost identical and quite small (less than 0.5 %).

With the data set from Haberschill et al. [27], the average absolute deviation of the COP and entrainment ratio is 9.23 % and 2.44 % for the constant pressure mixing model. For the variable pressure mixing model, the corresponding values are 8.55 % and 2.93 %. The variance is still low, with 0.5 % for COP and 0.04 % for entrainment ratio. In general, the accuracy of the two models are quite close. The Variable pressure mixing model is more accurate in the COP prediction whereas the constant pressure mixing model has a subtle advantage in the entrainment ratio prediction.

Fig. 14 to Fig. 15 describe the deviation of the vapor quality and the pressure at the ejector outlet. Since both of the parameters remain unchanged after post-processing of the data, only the validation results after data post-processing are presented. As shown in the figures, both models are more accurate in predicting the

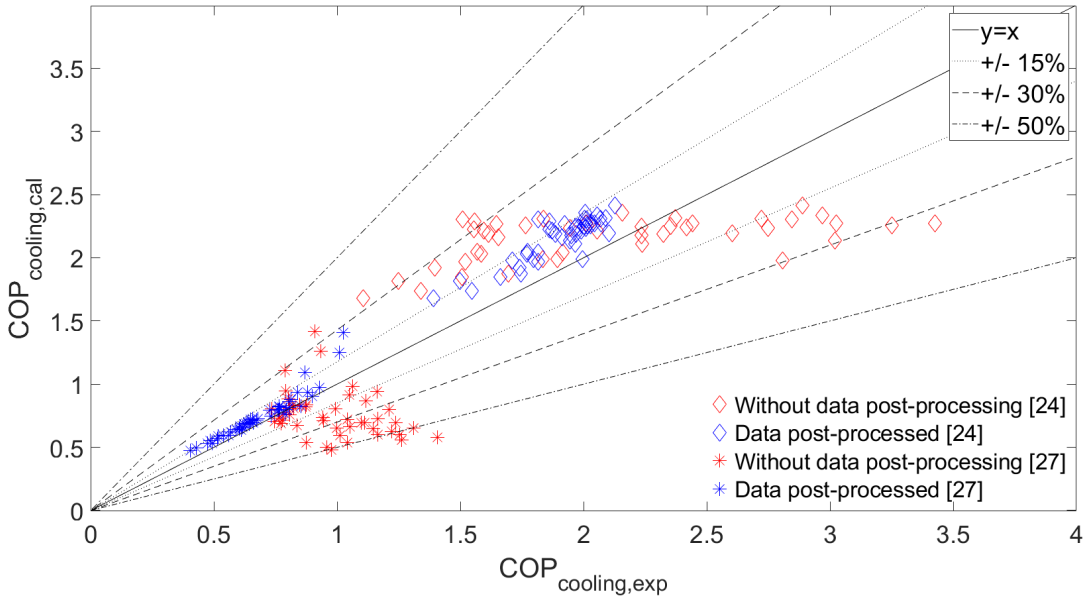

Figure 10: Simulated COP as a function of the experimental COP for the constant pressure mixing model [9]

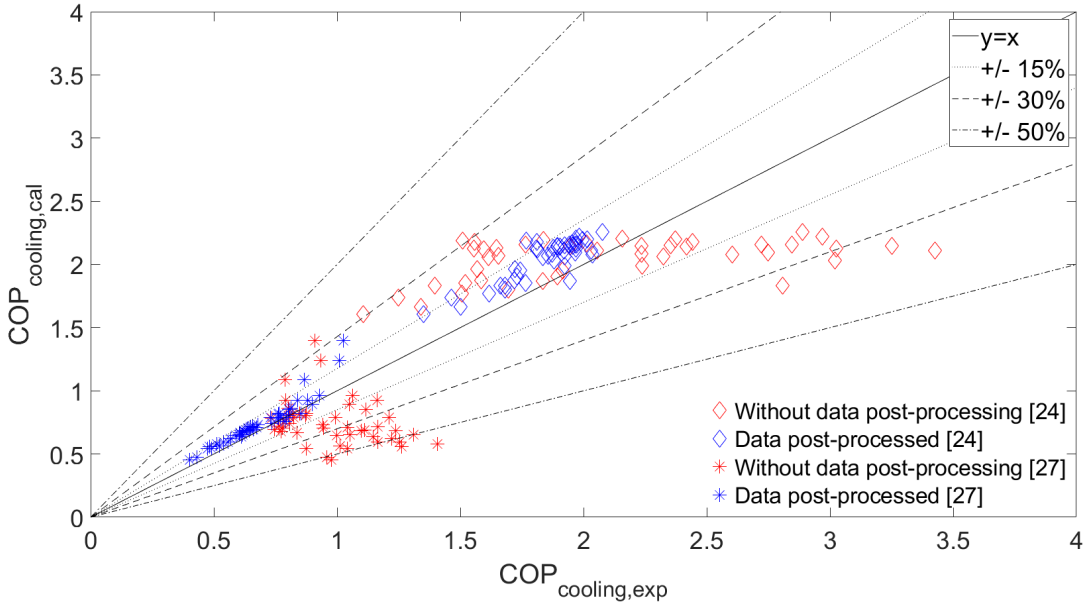

Figure 11: Simulated COP as a function of the experimental COP for the variable pressure mixing model [17]

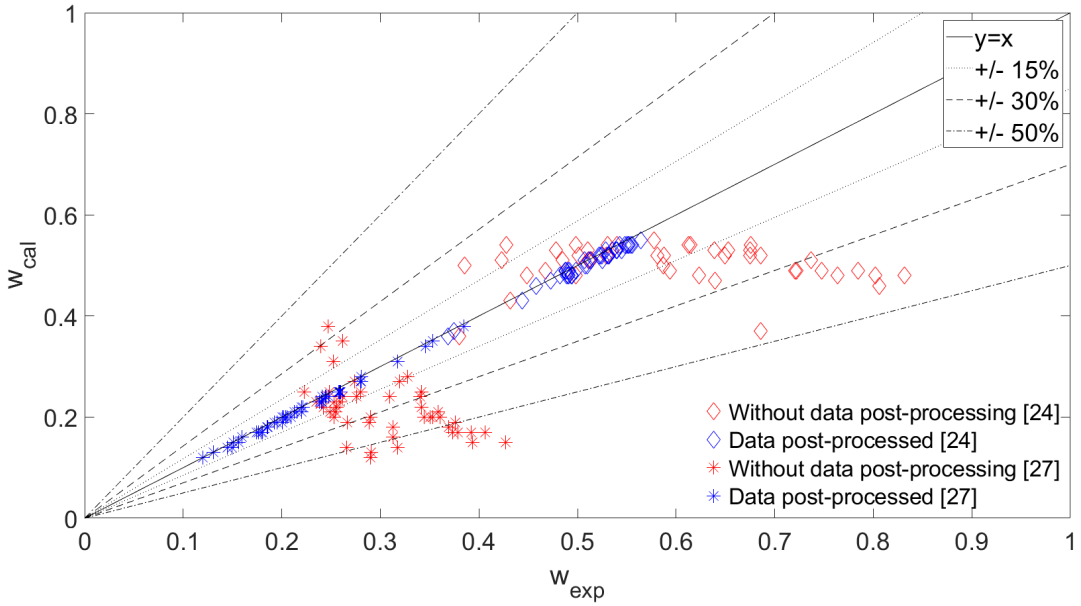

Figure 12: Calculated entrainment ratio versus experimental entrainment ratio for the constant pressure mixing model [9]

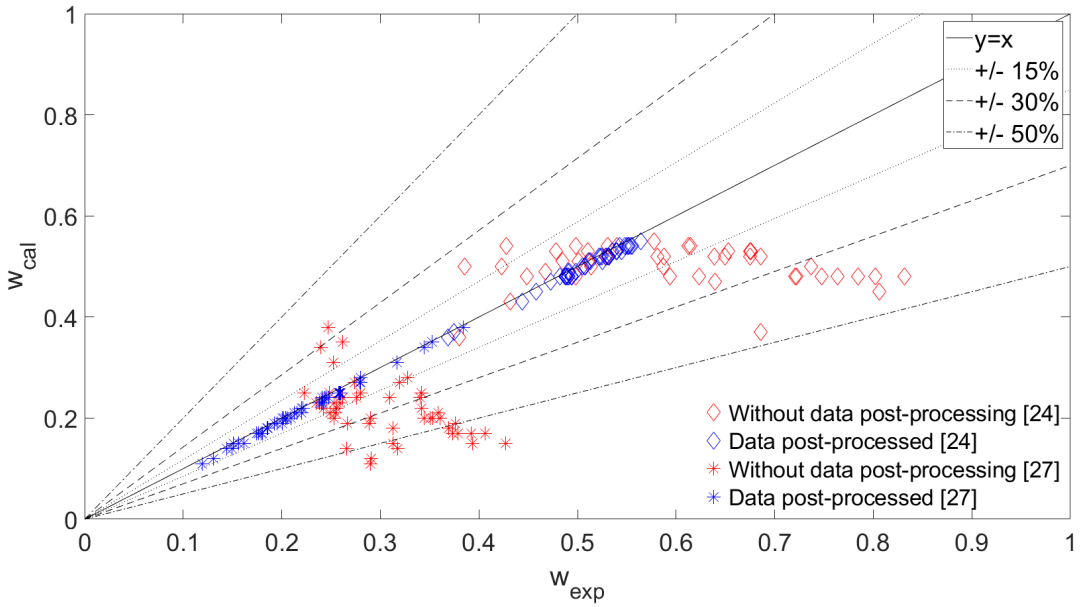

Figure 13: Calculated entrainment ratio versus experimental entrainment ratio for the variable pressure mixing model [17]

vapor quality and outlet pressure compared to the system COP and entrainment ratio of the ejector. The overall absolute relative error of the vapor quality is below 15%, and the simulation results match better with the experimental data from Haberschill et al. [27]. As to the outlet pressure of the ejector, the situation is reversed. The simulation results of the two 1-D models show better agreement with the data from Zhu et al. [24], and the deviation is generally less than 5 %.

Moreover, the simulated ejector outlet pressure is higher than the experimental value for the case of Haberschill et al. [27]. Comparing the two models, the accuracy of the prediction on the vapor quality and ejector outlet pressure is nearly identical. The difference of the average deviation is less than 0.6 %, except for the ejector outlet pressure in the case of Zhu et al. [24], where the average deviation is 2.99 % for the variable pressure mixing model and 0.84 % for the constant pressure mixing model.

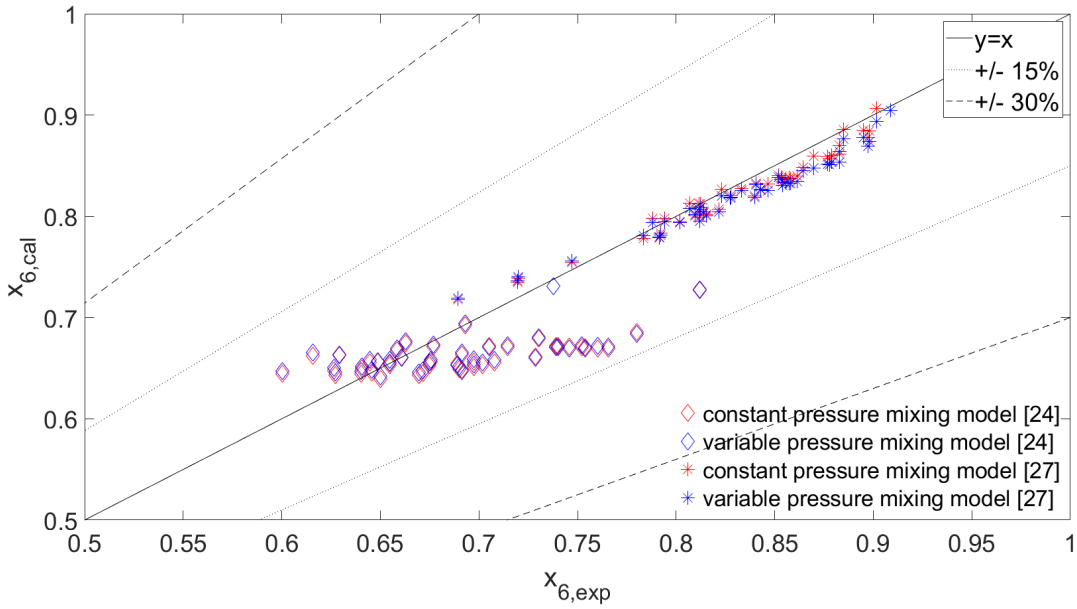

Figure 14: Calculated vapor quality versus experimental vapor quality at the ejector outlet

Based on the comparative analysis, conclusions can be drawn that both 1-D homogeneous equilibrium simulation models are able to predict the ejector outlet pressure and vapor quality precisely, but the simulated values for the entrainment ratio and the COP of the cycle have a large deviation from the original experimental data. When the models are validated with the processed experimental data, the deviation can be reduced to a reasonable range. A quantitative comparison of the two models shows that there is no notable difference in the prediction accuracy between the two models, which means neglecting the pressure variation during the mixing process has no effect on the model performance.

Conclusions

In this paper, two 1-D homogeneous equilibrium models of ejector expansion trancritical CO_2 heat pump cycle referred to [9, 17] were validated and compared with two independent experimental data bases [24, 27].

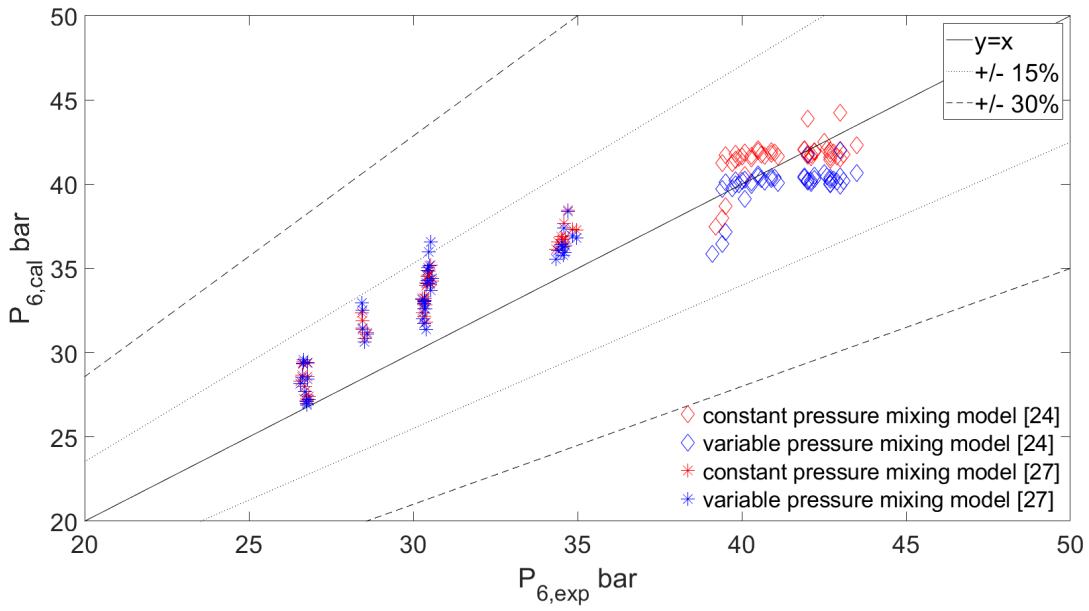

Figure 15: Calculated outlet pressure versus experimental outlet pressure of the ejector

A sensitivity analysis of the efficiency of the ejector components and the compressor was performed, and a post-processing method of the experimental data was proposed in order to verify the accuracy of the 1-D models in the ideal operating condition of the system. The main findings of this paper can be summarized as follow:

(1) Both 1-D homogeneous equilibrium models demonstrate accurate predictions of the ejector outlet pressure and vapor quality, with an overall deviation of less than 15%. However, for the cycle COP and the entrainment ratio of the ejector, a large deviation (more than 50%) is found if the actual system suffers from a liquid imbalance in the separator.

(2) A quantitative comparison of the two models shows that there is no major difference in prediction accuracy between the two models, which means neglecting the pressure variation during the mixing process has no effect on the model performance. Moreover, considering the complexity of the model and the solving time of the simulation, the constant pressure mixing model is a better choice.

(3) The liquid imbalance between the inlet and outlet of separator is a significant source of the modeling deviation. After eliminating the imbalance with an experimental data post-processing method, the error of COP can be reduced to less than 15% and the error of entrainment ratio is basically eliminated (less than 5 %).

(3) Compared to the isentropic efficincies of the ejector components, the system performance is more sensitive to the efficiency of the compressor. The method of calculating the compressor efficiency is critical to the accuracy of the 1-D homogeneous equilibrium models.

Acknowledgement

This work is supported by the funding of CETHIL, Institute National des Sciences Appliquees de Lyon (INSA-LYON, France) and the China Scholarship Council (CSC) [grant number 201806160297].

References

[1] A. T. Vekony, Heat pumps: 7 advantages and disadvantages, [EB/OL], `https://www.greenmatch.co.uk/` Updated September 07, 2019.

[2] B. T. Austin, K. Sumathy, Transcritical carbon dioxide heat pump systems: A review, Renewable and Sustainable Energy Reviews 15 (8) (2011) 4013–4029.

[3] M.-H. Kim, J. Pettersen, C. W. Bullard, Fundamental process and system design issues in CO_2 vapor compression systems, Progress in energy and combustion science 30 (2) (2004) 119–174.

[4] J. Sarkar, Ejector enhanced vapor compression refrigeration and heat pump systems—A review, Renewable and Sustainable Energy Reviews 16 (9) (2012) 6647–6659.

[5] A. A. Kornhauser, The use of an ejector as a refrigerant expander, International Refrigeration and Air Conditioning Conference, West Lafayette, Indiana, United States (1990).

[6] M. Ouzzane, Z. Aidoun, Model development and numerical procedure for detailed ejector analysis and design, Applied Thermal Engineering 23 (18) (2003) 2337–2351.

[7] J. Zhu, S. Elbel, Experimental investigation into the influence of vortex control on transcritical r744 ejector and cycle performance, Applied Thermal Engineering 164 (2020) 114418.

[8] J. Sarkar, Optimization of ejector-expansion transcritical CO_2 heat pump cycle, Energy 33 (9) (2008) 1399–1406.

[9] J. Deng, P. Jiang, T. Lu, W. Lu, Particular characteristics of transcritical CO_2 refrigeration cycle with an ejector, Applied Thermal Engineering 27 (2-3) (2007) 381–388.

[10] Y. He, J. Deng, Z. Zhang, Thermodynamic study on a new transcritical CO_2 ejector expansion refrigeration system with two-stage evaporation and vapor feedback, Hvac&R Research 20 (6) (2014) 655–664.

[11] Y. Song, Y. Ma, H. Wang, X. Yin, F. Cao, Review on the simulation models of the two-phase-ejector used in the transcritical carbon dioxide systems, International Journal of Refrigeration 119 (2020) 434–447.

[12] C. Lucas, H. Rusche, A. Schroeder, J. Koehler, Numerical investigation of a two-phase CO_2 ejector, International journal of refrigeration 43 (2014) 154–166.

[13] M. Colarossi, N. Trask, D. P. Schmidt, M. J. Bergander, Multidimensional modeling of condensing two-phase ejector flow, International journal of refrigeration 35 (2) (2012) 290–299.

[14] J. Smolka, Z. Bulinski, A. Fic, A. J. Nowak, K. Banasiak, A. Hafner, A computational model of a transcritical R744 ejector based on a homogeneous real fluid approach, Applied Mathematical Modelling 37 (3) (2013) 1208–1224.

[15] K. Ameur, Z. Aidoun, M. Ouzzane, Modeling and numerical approach for the design and operation of two-phase ejectors, Applied Thermal Engineering 109 (2016) 809–818.

[16] K. Banasiak, A. Hafner, T. Andresen, Experimental and numerical investigation of the influence of the two-phase ejector geometry on the performance of the R744 heat pump, International journal of Refrigeration 35 (6) (2012) 1617–1625.

[17] D. Li, E. A. Groll, Transcritical CO_2 refrigeration cycle with ejector-expansion device, International Journal of refrigeration 28 (5) (2005) 766–773.

[18] F. Liu, E. A. Groll, D. Li, Investigation on performance of variable geometry ejectors for CO_2 refrigeration cycles, Energy 45 (1) (2012) 829–839.

[19] S. W. Elbel, P. S. Hrnjak, Effect of internal heat exchanger on performance of transcritical CO_2 systems with ejector, International Refrigeration and Air Conditioning Conference, West Lafayette, Indiana, United States (2004).

[20] K. Banasiak, A. Hafner, 1d computational model of a two-phase R744 ejector for expansion work recovery, International Journal of Thermal Sciences 50 (11) (2011) 2235–2247.

[21] L. Zheng, J. Deng, Z. Zhang, Dynamic simulation of an improved transcritical CO_2 ejector expansion refrigeration cycle, Energy Conversion and Management 114 (2016) 278–289.

[22] F. Liu, E. A. Groll, Study of ejector efficiencies in refrigeration cycles, Applied Thermal Engineering 52 (2) (2013) 360–370.

[23] K. Chunnanond, S. Aphornratana, An experimental investigation of a steam ejector refrigerator: the analysis of the pressure profile along the ejector, Applied thermal engineering 24 (2-3) (2004) 311–322.

[24] Y. Zhu, C. Li, F. Zhang, P.-X. Jiang, Comprehensive experimental study on a transcritical CO_2 ejector-expansion refrigeration system, Energy Conversion and Management 151 (2017) 98–106.

[25] M. Nakagawa, A. Marasigan, T. Matsukawa, A. Kurashina, Experimental investigation on the effect of mixing length on the performance of two-phase ejector for CO_2 refrigeration cycle with and without heat exchanger, International Journal of Refrigeration 34 (7) (2011) 1604–1613.

[26] F. Aligolzadeh, A. Hakkaki-Fard, A novel methodology for designing a multi-ejector refrigeration system, Applied Thermal Engineering 151 (2019) 26–37.

[27] P. Haberschill, E. Nehdi, L. Kairouani, M. A. Elakhdar, Experimental study of a two-phase ejector for CO_2 transcritical refrigeration system, Archives of Thermodynamics (2021) 217–246.

Appendix

A. Reproduction of the ejector expansion refrigeration models

Fig. A1 to Fig. A5 shows the simulation results of the reproduced models [9, 17] compared to the original simulation data in their articles (both models are only theoretical studies and have not been experimentally verified in the original work). During the reproduction, the input isentropic efficiencies of the ejector components and the compressor are identical to the original work.

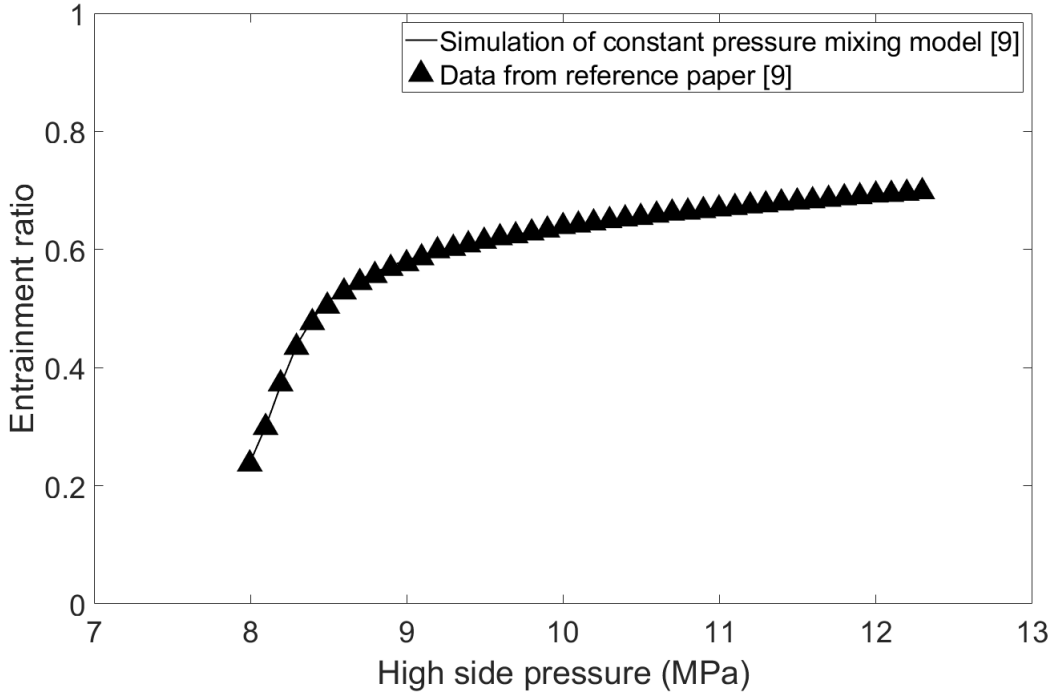

Figure A1: Entrainment ratio as a function of compressor discharge pressure

$T_{gc,o} = 36\ °C$, $T_e = 5\ °C$, $T_{sh} = 0\ °C$

$\eta_m = 0.7,\ \eta_d = 0.8,\ \eta_{comp} = 1.003 - 0.121 \cdot (P_m/P_s)$

For the constant pressure mixing model, the entrainment ratio of the ejector rises with high-side pressure, and the trend of ejector outlet vapor quality is reversed due to the link $(1 + w) \cdot x = 1$. The COP increases first then starts to decrease at certain point. The COP arrives the highest value, which means the optimum cycle performance when the entrainment ratio is between 0.5 to 0.6.

For the variable pressure mixing model, an extra evaluation parameter R is introduced, which is the ratio between the COP of ejector expansion cycle and COP of basic heat pump cycle without ejector. Different pressure drops in the suction nozzle are studied. R decreases with the entrainment ratio and increase with higher pressure drop in the suction nozzle. R increases with the high-side pressure before reaching a specific point, where continuing to increase the pressure does not improve the R value. For a particular high-side pressure, raising the entrainment ratio will improve the performance of the ejector expansion heat pump cycle.

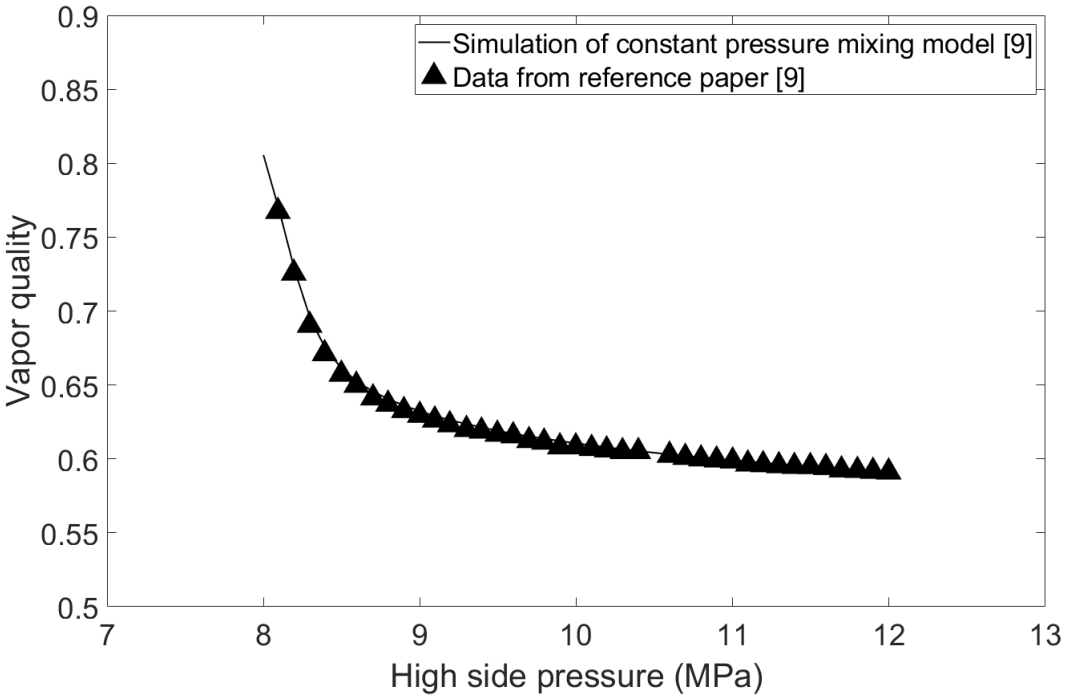

Figure A2: Vapor quality as a function of compressor discharge pressure

$T_{gc,o} = 36\ ^\circ C$, $T_e = 5\ ^\circ C$, $T_{sh} = 0\ ^\circ C$

$\eta_m = 0.7,\ \eta_d = 0.8,\ \eta_{comp} = 1.003 - 0.121 \cdot (P_m/P_s)$

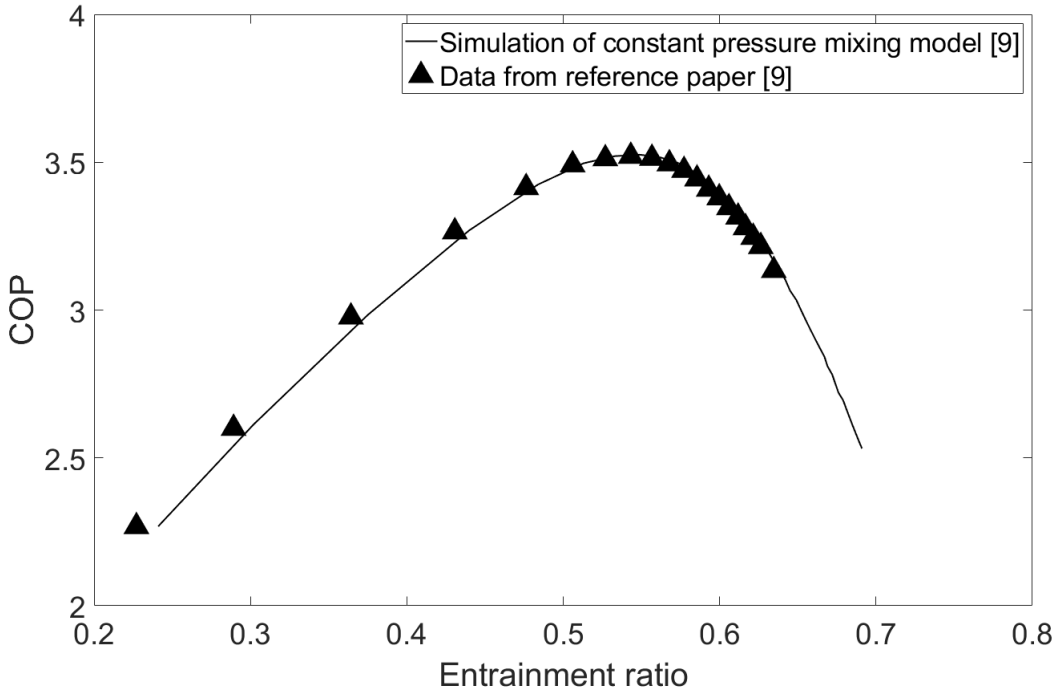

Figure A3: COP as a function of entrainment ratio of the ejector

$T_{gc,o} = 36\ ^\circ C$, $T_e = 5\ ^\circ C$, $T_{sh} = 0\ ^\circ C$

$\eta_m = 0.7,\ \eta_d = 0.8,\ \eta_{comp} = 1.003 - 0.121 \cdot (P_m/P_s)$

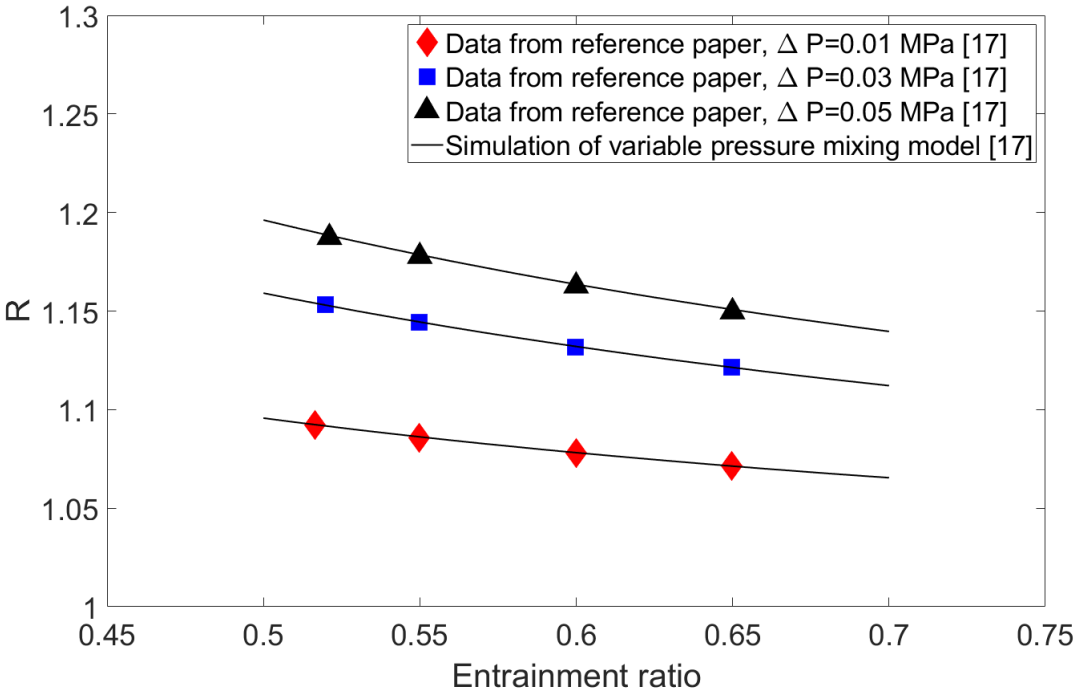

Figure A4: Relative performance ratio versus entrainment ratio and pressure drop

$T_{gc,o} = 40\ ^{\circ}C$, $T_e = 5\ ^{\circ}C$, $T_{sh} = 5\ ^{\circ}C$

$\eta_m = 0.9,\ \eta_s = 0.9,\ \eta_d = 0.8,\ \eta_{comp} = 0.75$

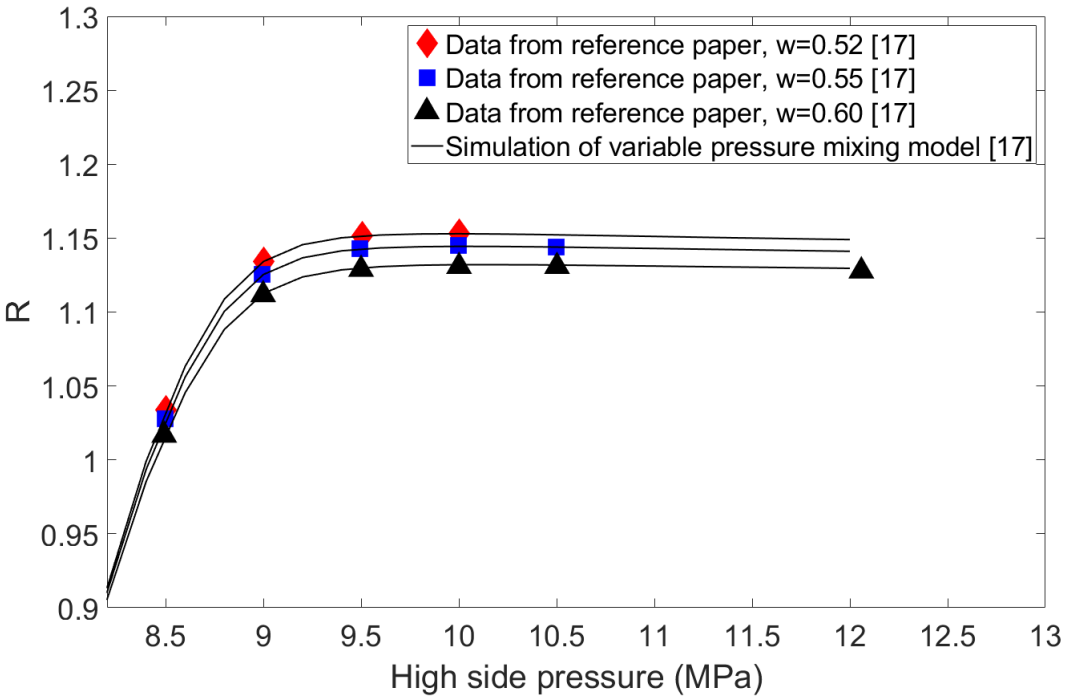

Figure A5: Relative performance ratio versus high-side pressure and entrainment ratio

$\Delta P = 0.03\ MPa$, $P_{gc,o} = 10\ MPa$, $T_{gc,o} = 40\ ^{\circ}C$, $T_e = 5\ ^{\circ}C$, $T_{sh} = 5\ ^{\circ}C$

$\eta_m = 0.9,\ \eta_s = 0.9,\ \eta_d = 0.8,\ \eta_{comp} = 0.75$